Contents lists available at ScienceDirect

Journal of Magnetism and Magnetic Materials

Soft and hard natures of $Nd_2Fe_{14}B$ permanent magnet explored by first-order-reversal-curves

Po-An Chen [a], Chao-Yao Yang [a], Shu-Jui Chang [a], Min-Han Lee [b], Nai-Kuang Tang [c], Sheng-Chan Yen [c], Yuan-Chieh Tseng [a,*]

[a] *Department of Materials Science & Engineering, National Chiao Tung University, Hsinchu, Taiwan, ROC*
[b] *Undergraduate Honors Program of Nano Science & Engineering, National Chiao Tung University, Hsinchu, Taiwan, ROC*
[c] *Metal Industries Research and Development Center, Kaohsiung, Taiwan*

A B S T R A C T

Two commercial $Nd_2Fe_{14}B$ samples, MQP-B and sintered-NdFeB were investigated using synchrotron-based x-ray diffraction and first-order-reversal-curves (FORCs). Despite differing in magnetic and structural properties, the two samples were found to comprise two major ferromagnetic components in FORCs. For the sintered-NdFeB case, the soft component may originate from the intrinsically soft Nd-f site which was coupled with its local Fe atomic environment that differs in magnetic anisotropy from the Nd-g site (intrinsically hard). It may directly originate from the Nd-rich phase or microstructural imperfection, while the former possibility (Nd-f site) appears greater than the latter. While for the MQP-B, the minor second phase resulting from high structural disorder was likely in charge of the presence of the soft component. Sophisticated FORCs analyses revealed the natures of the soft and hard components, soft–hard coupling and switching reversibility of the two cases, irrespective of the origins of their two components. This provides insights to the origin of magnetic stability and reversal dynamics of $Nd_2Fe_{14}B$ that have not been fully understood by conventional magnetic analyses. The coexistence of the two components led to an incoherent reversal undermining the magnetic stability of $Nd_2Fe_{14}B$. This is a fundamental problem as to why the performance extremity can only be improved finitely through extrinsic tuning. From FORCs simulation we understand that the soft–hard coupling was moderate in a real $Nd_2Fe_{14}B$ compound. A stronger soft–hard coupling is necessary to conquer the anisotropic competition to enable a coherent reversal that will promote the magnetic hardness.

© 2014 Elsevier B.V. All rights reserved.

1. Introduction

$Nd_2Fe_{14}B$ is thought of as the best permanent magnetic material available today, owing to its large magnetic energy product ($(BH)_{max}$) that possesses wide applications in micromagentic devices and permanent magnetic motors [1,2]. The magnetic hardness (coercivity, H_c) is mainly dominated by Nd ions located in two inequivalent crystallographic sites within the tetragonal structure [3,4]. The saturation magnetization (M_s) of the compound primarily arises from Fe ions ($31\mu_B$ for Fe and $6\mu_B$ for Nd per formula unit) [3]. The product of H_c and M_s defines the $(BH)_{max}$ and determines the ultimate applicability of the compound. Numerous studies have focused on the influences of grain-size [5–7], atomic substitutions [8–11] and microstructural modifications [12–15] on $(BH)_{max}$, yet the performance of the

compound appears to have reached the limitation through extrinsic tuning. From a fundamental aspect perhaps exploring the unknown properties of the $Nd_2Fe_{14}B$ with modern techniques could open more opportunities to pushing the performance extremity of such a venerable permanent magnet, which is the motivation of this study.

First-order-reversal-curves (FORCs) is a new tool for characterizing the hysteretic dependence of materials [16–20]. The tremendous amount of information such as a full mapping of magnetic switching, coexistence of soft and hard magnetic natures, and the distribution of interaction field between magnetic units can be visualized through FORCs, rather than simply estimating the parameters of M_s, H_c and M_r (remanent magnetization) from a major hysteresis loop. In this study we applied FORCs analysis to two commercially available $Nd_2Fe_{14}B$ samples to explore their unknown properties. We found that though they differ markedly in magnetic/structural properties, both samples consisted of soft and hard ferromagnetic (FM) components in FORCs distributions, which was unexpected from a "hard" permanent magnet. The

* Corresponding author.
E-mail address: yctseng21@mail.nctu.edu.tw (Y.-C. Tseng).

coexistence of the two components caused incoherent responses in magnetization reversal. With FORCs simulations we estimated the interaction strength between the soft and hard components to acquire how the soft–hard dependency mediated the switching coherency. The results showed that the coupling between the two components was rather moderate in a real $Nd_2Fe_{14}B$ compound, and enhancing the coupling was critical to enable a coherent reversal that would effectively improve the magnetic stability of the $Nd_2Fe_{14}B$.

2. Experimental details and methods

Two commercially available $Nd_2Fe_{14}B$ samples were used in this study. The first commercial MQP-B (intrinsic $H_c = 3.50$ kOe) powders supplied by Magnequench Int. Inc., were rapidly solidified from the molten state with a cooling rate of 10^6 K/s and were heat treated at 600 °Cfor 3 min. We were informed that the MQP-B sample has a grain size of 30 nm in diameter. The second

commercial sample supplied by the local vender, defined as sintered-NdFeB thereafter, was first prepared by strip casting technique. After hydrogen decrepitation (HD) process, the cast strips were pulverized into fine powders. The as-cast strips were sintered at 1100 °C for 2 h in an Ar atmosphere, and were subsequently subjected to further thermal treatments, being first heat-treated at 900 °C for 30 min and then followed by another treatment of 550 °C for 4 h. About ~3% of Cr and Zr were added to enhance the chemical stabilities of the MQP-B and sintered-NdFeB, respectively. The stoichiometry of the two samples was determined by inductively coupled plasma mass spectrometry (ICP-MS) as detailed in Table 1. Powder x-ray diffraction (XRD) measurements were performed at the BL01C2 of the National Synchrotron Radiation Research Center, Taiwan, with an x-ray energy of 25 keV. The two samples were ground into fine powders and were sieved by a 75 µm mesh to exclude the particle-size effects from XRD characterizations. Rietveld refinement was used to construct standard $Nd_2Fe_{14}B$ $P4_2/mnm$ crystallographic structure to fit the experimental XRD. For magnetic characterizations, the two powder samples were prepared into identical bulk forms with a non-magnetic varnish to prevent the rotation of the powders during the vibrating sample magnetometer (VSM) measurements. First-order-reversal-curves (FORCs) were collected using a VersaLab VSM (Quantum Design manufacture) with an auto-run script programmed by the Visual-Basic software. During measurements, the magnetization was measured starting from a reversal field after saturation, defined as H_r, back to the positive saturation to produce a FORC. A family of FORCs was obtained with different H_r but equal field spacing that filled the interior of the major hysteresis loop. According to the classical Preisach model [21,22]

Table 1
ICP-MS results on MQP-B and sintered-NdFeB.

Element	MQP-B (at%)	Sintered-NdFeB (at%)
Nd	11.58	15.53
Fe	80.06	76.43
B	5.50	5.24
Cr	2.86	
Zr		2.80
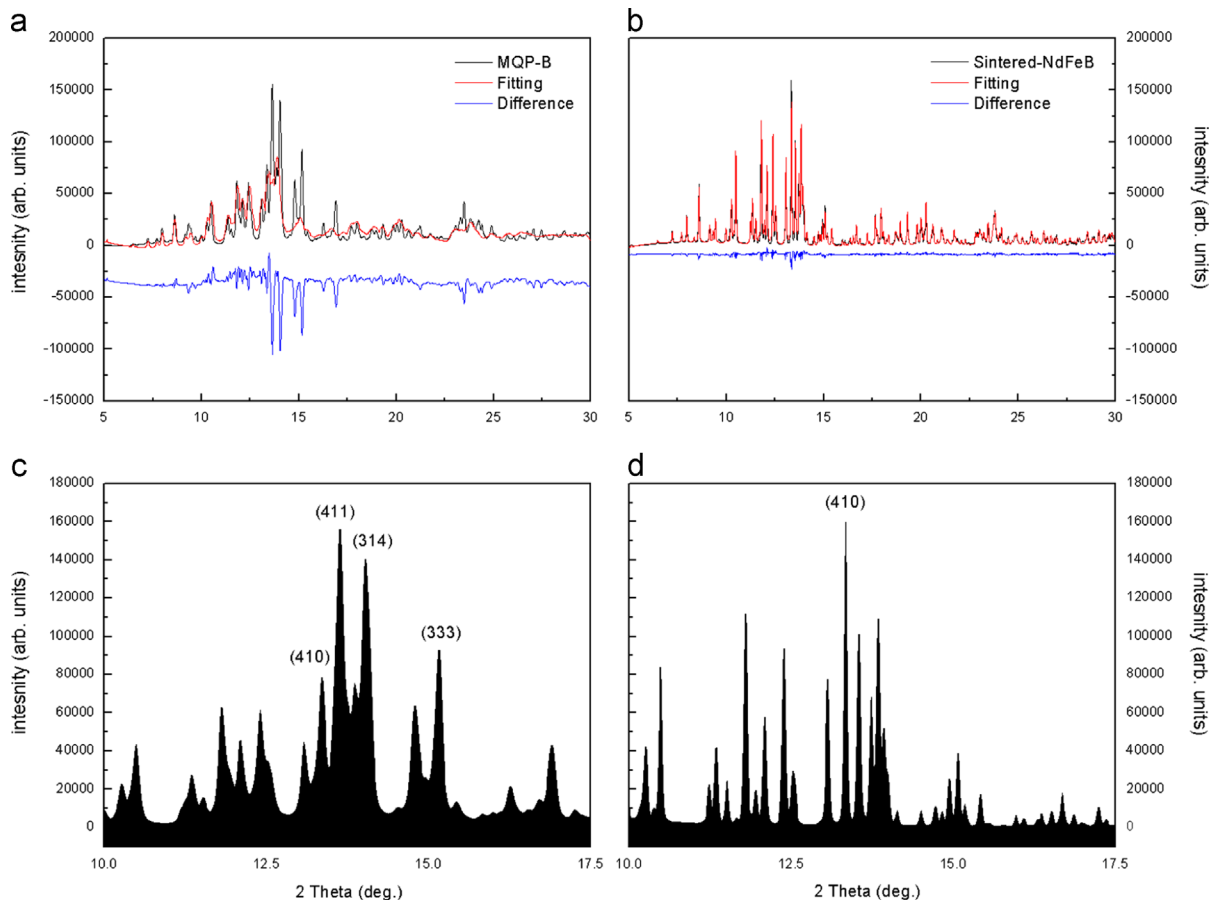
Fig. 1. XRD patterns and corresponding rietveld refinements of the (a) MQP-B and (b) sintered-NdFeB. (c) and (d) show the partially indexed XRDs for the MQP-B and sintered-NdFeB, respectively for the comparison in crystallographic texture.

the FORCs distribution is defined as follows:

$$\rho(H_a, H_r) = -\frac{1}{2}\frac{\partial^2 m(H_a, H_r)}{\partial H_a \partial H_r}$$

where H_a is the applied field and m is the measured magnetization of the material. The field intervals of H_a and H_r for the FORCs measurements of the two samples were both 197 Oe. Using a home-made python program, the FORCs diagrams were transformed into in 2-dimensional (2-D) and 3-dimensional (3-D) contour plots by mathematically converting the coordination from H_r/H_a into H_b/H_c, using the equations of $H_c=(H_a-H_r)/2$ and $H_b=(H_a+H_r)/2$. Details about the FORCs analysis can be found in Ref. [16–18]. FORCs simulations were carried out by a python program, with details described in the content. Since the two bulk samples were prepared from powders, the FORCs measurements were not bothered by the intrinsic anisotropic effects of the samples when they were put into comparison.

3. Results and discussion

Fig. 1(a) and (b) shows the experimental XRD patterns along with the Rietveld refinements of the MQP-B and sintered-NdFeB, respectively. The sintered-NdFeB exhibits a clear tetragonal structure highly consistent with the theoretical model. The MQP-B is characteristic of peak-broadening in XRD, suggesting structural disorder arising from the extremely fast cooling rate that had failed to develop a clear tetragonal phase. Fig. 1(c) and (d) shows the partially indexed XRDs of the MQP-B and sintered-NdFeB, respectively. According to literature [23], the (410) has the strongest intensity for the isotropic raw material. Therefore, from Fig. 1(c) and (d) we understand that the crystallographic texture of the sintered-NdFeB is close to isotropic due to the strongest (410) and narrow width of the XRD peaks. For the MQP-B, the much reduced (410) in comparison to stronger (411), (314) and (333) suggests anisotropic texture along the (411), (314) and (333) planes. As the XRD peaks are quite broadened in the MQP-B, the textured planes are expected to be with small grain size. The MQP-B yields a saturation magnetization (M_s) of 670 emu/cm^3, a remanent magnetization (M_r) of 330 emu/cm^3, and an H_c of 3500 Oe. In contrast, an M_s of 1200 emu/cm^3, an M_r of 960 emu/cm^3, and an H_c of 11,000 Oe are produced by the sintered-NdFeB. The M_s, M_r, and H_c of the sintered-NdFeB are slightly smaller, but still in a close proximity to those employing a similar annealing process [24,25]. The shoulders present at low fields of the sintered-NdFeB are attributed to the irregular domain configurations at the bulk surface, as these features are absent to the powder form. Fig. 2(a) presents the B–H curves of the two samples converted from their M–H curves, producing $(BH)_{max}$ of 3.5 and 42.6 MGOe for the MQP-B (Fig. 2(c)) and sintered-NdFeB (Fig. 2(d)), respectively. We conclude that the much more pronounced $(BH)_{max}$ of the sintered-NdFeB than the MQP-B has be due to a higher structural stability, isotropic texture, and a prolonged heat treatment. At an atomic scale, a higher structural stability especially along the [110] and [001] directions is expected to
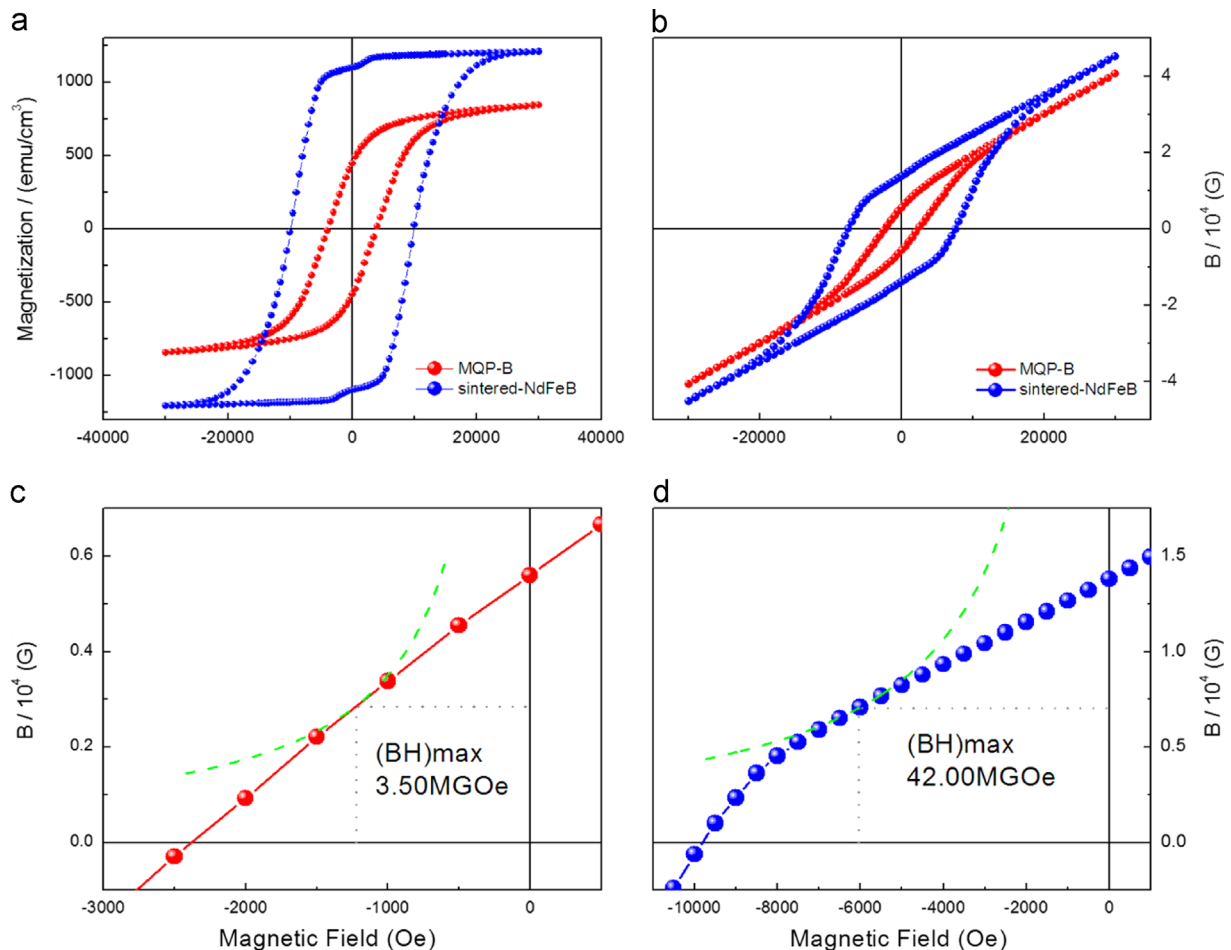

Fig. 2. (a) M–H curves and (b) B–H curves of the MQP-B (red) and sintered-NdFeB (blue). (c) and (d) are the $(BH)_{max}$ estimations of the MQP-B and sintered-NdFeB, respectively. The horizontal axes of all sub-figures are scaled by magnetic fields in Orsted (Oe) but with different ranges. (For interpretation of the references to color in this figure legend, the reader is referred to the web version of this article.)

stabilize the Nd alignments directly favoring the magneto-crystalline anisotropy (MCA) as well as H_c. It also stabilizes the Fe atomic environments around the Nd ions, thereby promoting the saturation magnetization by facilitating Fe $3d$–Nd $4f$ exchange interactions.

Fig. 3(a) and (b) presents the raw FORCs measurements of the MQP-B and sintered-NdFeB, respectively. Fig. 3(c) and (d) is the converted FORCs 2-D contour diagrams corresponding to Fig. 3 (a) and (b), respectively. More details on the intensity distributions can be acquired in the 3-D FORCs contour diagrams of Fig. 3(e) and (f) corresponding to Fig. 3(a) and (b), respectively, at which the intensity reflects the number of hysteron [16,26]. The magnetization has been normalized to M_s in both Fig. 3(a) and (b), so the intensity scale presented in Fig. 3(c)–(f) is all in a relative manner. Besides, we adopted extrapolated FORCs method suggested by Béron et al. [27] to extract the nonperturbed traces of the small-H_c component of the MQP-B. This method is more reliable for small-H_c FORCs in comparison to the the relaxed-fit [28] and reversible-ridge [29] methods as it minimizes the discontinuities near $H = H_r$. In Fig. 3(c) and (d), the two samples both present a two-peak distribution, indicating the coexistence of two major reversal components. The one located at the low H_c can be thought of as a soft ferromagnetic component, while the other with the center

located at a larger H_c is a hard ferromagnetic component. The soft and hard centers are found to locate at 150 and 5900 Oe, respectively for the MQP-B, but are positioned at 4700 and 12,800 Oe, respectively for the sintered-NdFeB.

The MQP-B and sintered-NdFeB appear to differ in many ways in terms of structural (XRD, Fig. 1) and magnetic (Fig. 2) properties due to different fabrication details, whereas they both consist of soft and hard components. Especially for the sintered-NdFeB, the found FORC distribution is quite similar to Schrefl et al. [30] showing more than one distribution. Though there are several studies suggesting that the soft component may originate from α-Fe and FeB phases unexpectedly produced in sample preparation [31–34], it is important to be reminded that, whether the removal of these second phases would lead to a single hard magnetic phase is never validated. Microstructural imperfections at the grain boundaries, as pointed out by Bance et al.[35] are likely responsible for the soft features observed in FORCs. Nevertheless, the soft component might be intrinsic in the sintered-NdFeB based on the three arguments. First, the soft α-Fe and FeB phases are not identified by the XRD of the sintered-NdFeB as the structure is well fitted by the theory, but the soft component is still observed in its FORCs. From stoichiometric analyses (Table 1), it is
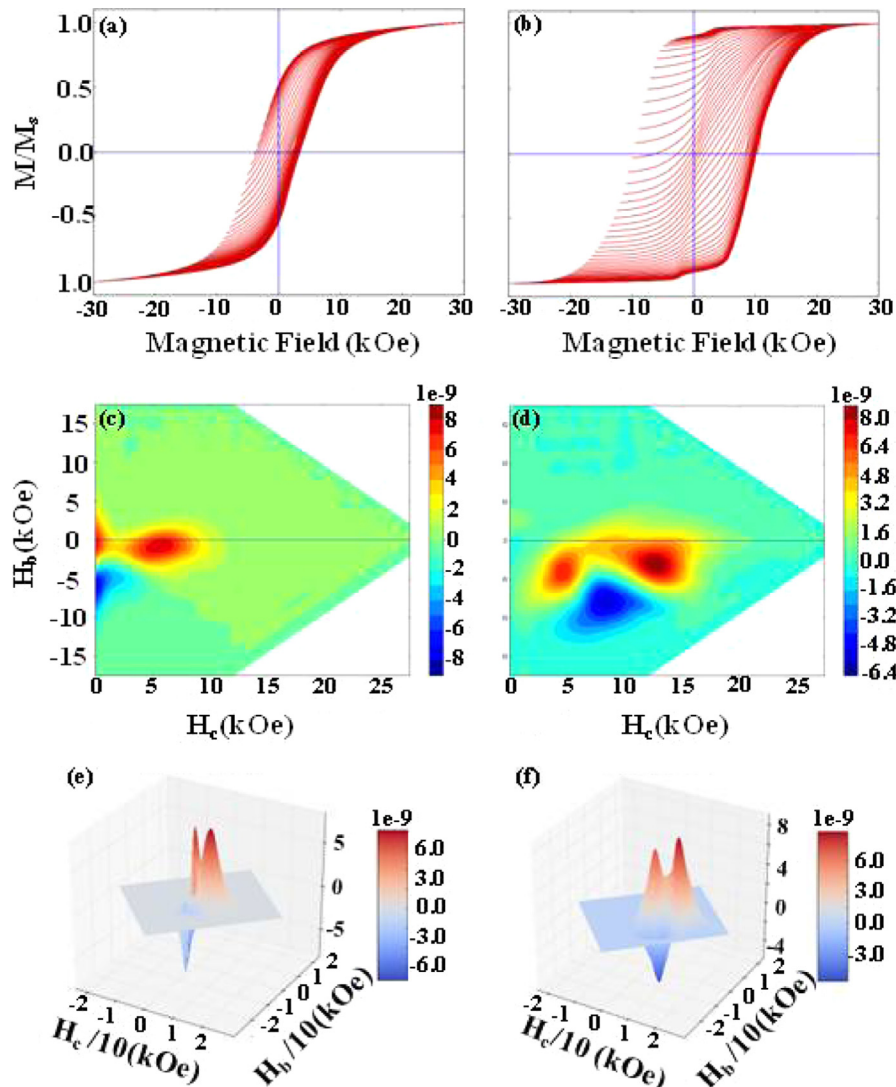

Fig. 3. (a) and (b) are original FORCs of the MQP-B and sintered-NdFeB, respectively. (c) and (d) are the converted 2-D contours with H_b and H_c scales, which correspond to (a) and (b), respectively. (e) and (f) are the converted 3-D contours correspond to (a) and (b), respectively, with the addition of the intensity scale with respect to H_b and H_c. (a) and (b) share the same vertical scale in M/M_s, and (c) and (d) share the same vertical scale in H_b (kOe).

clear that the sintered-NdFeB contains Nd-rich phases that may be in charge of the presence of the soft component. However, even if there exists Nd-rich phase at gran-boundaries in this high $(BH)_{max}$ sample, such second phase is more associated with a hard phase which is often created intentionally during fabrication to increase the coercivity [36–38]. Second, the soft component could be introduced from unavoidable oxidation in sample preparation, or the addition of Cr, Zr, Al or Ni elements (only a few percent) for the purpose of enhancing the chemical stability. Nevertheless, the soft component with an H_c as large as $\sim$4700 Oe is unlikely to be created simply via light oxidation or low-doping. An H_c of $\sim$4700 Oe, in fact, should be regarded as a hard magnetic nature by definition [39], but we define it as soft simply because of the presence of a harder component. From 3-D FORCs the number of the soft hysterons is with the same order of magnitude to that of the hard ones, and their overlapping (coupling) is notable. This implies that the two components present intrinsically and influence each other through interior interactions. Third, there are several studies reporting the enhanced magnetic properties from a nano-composite process [34,40–43]. With such fabrication the exchange interactions can be initiated between the extrinsic soft (usually created by the addition of transition metals or refractory elements) and the intrinsic hard ($Nd_2Fe_{14}B$) components across grains with the size smaller than 20 nm. However, our samples were free from the nanocomposite process and, the grain size (in a few (2–3) micrometers) of the sintered-NdFeB appears to exceed the critical exchange length. Therefore, even if there presents any unexpected extrinsic soft component, the exchange interactions are unlikely to be triggered to a level similar to the soft–hard coupling observed in the FORCs. Summarizing the above information, we conclude that for the sintered-NdFeB, the soft component could either be intrinsic or extrinsic (originate from the Nd-rich phase), but the latter one seems to be not very evident. Of course an extremely high quality, second-phase free sample is very necessary to better identify the soft-component of this permanent magnet.

The discovery of different intrinsic magnetic stabilities for two inequivalent Nd sites by Haskel et al. [4] provides a more plausible mechanism for our finding, where the magnetic hardness of the $Nd_2Fe_{14}B$ is found to arise predominately from the g site Nd ions, but the f site Nd ions reduce the intrinsic stability with a smaller H_c. However, differing from Haskel et al. [4] directly probing the two Nd sites using x-ray scattering, FORCs distributions were constructed by probing the magnetization change of the entire sample, which is more associated with the contributions from Fe. Therefore, the soft and hard components may likely originate from the two Nd sites in the sintered-NdFeB, with large magnetic backgrounds given by the respective Fe atomic environments that hybridized with Nd. The magnetic structure of $Nd_2Fe_{14}B$ at room temperature, together with the individual hysteresis loops of the two Nd sites (figure cited from Haskel et al. [4]) probed by x-ray scattering, are provided in Fig. 4(a) and (b), respectively. Considering that the Nd–Nd coupling is indirect and weak due to localized $4f$ orbital [44], the coupling between the two components must be initiated through the Nd–Fe and Fe–Fe direct exchange. For the sintered-NdFeB, the hard component dominates the magnetization reversal by having a more broadened distribution along with a stronger intensity (a larger number of hysteron) than the soft one. This is somehow supported by Haskel et al. [4] emphasizing the dominance of the g site Nd on the MCA while effect of the f site Nd is opposite and secondary. Yet differing from Haskel et al. [4] the dominance of the hard component in the FORCs cannot be solely attributed to the g site Nd alone, but rather the vigorous Fe–Nd exchange interactions around the g site Nd. Another fact pointing to the dominance of the hard component in the sintered-NdFeB can be examined from the major hysteresis loop, which yields an H_c of $\sim$11,000 Oe rather close to its hard component center at 12,800 Oe. In contrast, in the MQP-B the FORCs intensity of the hard component is reduced to a level comparable to that of the soft component. This can be explained as the deterioration from the structural disorder, which has smeared the structural symmetry disfavoring the MCA and the coupled magnetic stability, therefore losing the dominance as opposed to that obtained in the sintered-NdFeB. In this case both components are suppressed profoundly in comparison with the sintered-NdFeB. If one weights the H_c of the two components of the MQP-B equally, it will produce an H_c of $\sim$3000 Oe fairly close to 3500 Oe directly gained from the major hysteresis loop. This means that the two components of the MQP-B are rather close in terms of domination. The origin of the soft component in the MQP-B is more likely related to the second phases resulting from highly disordered structure, instead of the Nd-f site. These second phases are intimately connected to anisotropic textures along the (411), (314) and (333) planes.

Understanding the switching behaviors is essential to the developments of modern magnetic materials, and this can be
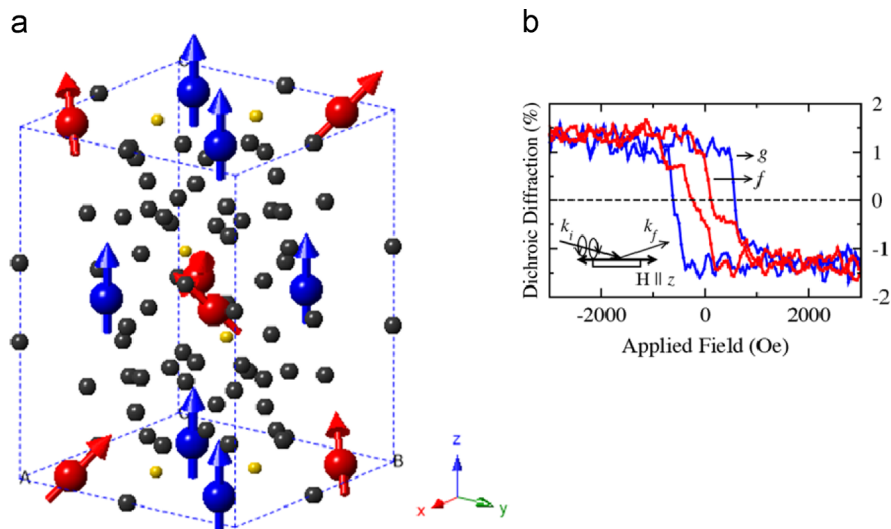
Fig. 4. (a) Magnetic structure of the $Nd_2Fe_{14}B$ tetragonal phase at room temperature with the magnetic field applied along the c-axis. Blue and red balls represent the Nd g and Nd f sites, respectively. Black and yellow balls represent the Fe and B atoms, respectively. The illustration was built based on the finding of Haskel [4]. (b) Resonant magnetic scattering of the two Nd sites (blue for g site and red for f site) showing individual hysteresis loops. Figure is cited from Haskel [4]. (For interpretation of the references to color in this figure legend, the reader is referred to the web version of this article.)

done by properly analyzing the FORCs data. In FORCs a hysteron represents a single, smallest switchable magnetic unit, and a reversible switch is defined as that such a magnetic unit can fully return to the initial path of the major loop at a given H_r [45]. Fig. 5 illustrates the inter-relations between the reversible and irreversible components (only qualitative) with respect to a single FORC near H_r. Using the methods of Winklhofer et al. [45] we were able to quantitatively extract the reversible and irreversible components of the MQP-B and sintered-NdFeB from their FORCs diagrams, and their distributions are presented in Fig. 6(a) and (b),
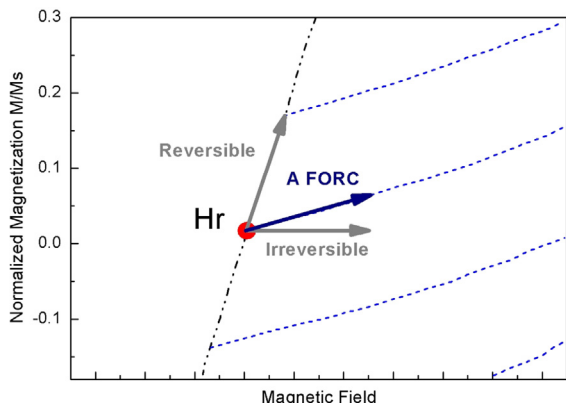

Fig. 5. A zoomed-in FORCs diagram illustrating the inter-relations between the reversible and irreversible components near H_r (red point). Black and blue dashed lines represent the partial curves of the major hysteresis loop and FORCs, respectively. (For interpretation of the references to color in this figure legend, the reader is referred to the web version of this article.)

respectively. The decomposing of reversible and irreversible processes was operated near the descending branch of the major loop by monitoring the magnetization change versus H_r in the original FORC; i.e., dM/dH_r. In mathematics the reversible/irreversible decomposing can be summarized by the equations as follows [45]:

$$dM^{irr}(H_r) = \lim_{H_a \to H_r} [M(H_a) - M(H_r, H_a)]$$

$$dM^{rev}(H_r) = \lim_{H_a \to H_r} [M(H_r, H_a) - M(H_r)]$$

In Fig. 6(a), the MQP-B displays comparable reversible and irreversible contributions. Conversely, a large irreversible contribution coupled with a greatly suppressed reversibility is observed in the sintered-NdFeB (Fig. 6(b)). This indicates that the switching mechanism of the sintered-NdFeB is highly irreversible. In principle, integrations of the dM/dHr curves could quantitatively reflect the involved magnetic entities during a reversible or irreversible process. This means that the sintered-NdFeB requires extra fields to rotate the tremendous amounts of irreversible components to complete a magnetization reversal. We further construct the purely reversible and irreversible parts of the major loop for the MQP-B and sintered-NdFeB in Fig. 6(c) and (d), respectively. The data are presented by magnetization (scale up to 1.0) as a function of H_r. By a rough estimation we understand that the major loop of the MQP-B is contributed evenly by the reversible and irreversible loops. Nevertheless, the irreversible loop of the sintered-NdFeB almost scales with the major loop (Fig. 3(b)), but the reversible loop only plays a very minor role in the global properties. In general, a hard magnet is expected to be more irreversible than a soft magnet, because the former is more resistant to the field reversal with the strong MCA. However, the reversibility of the
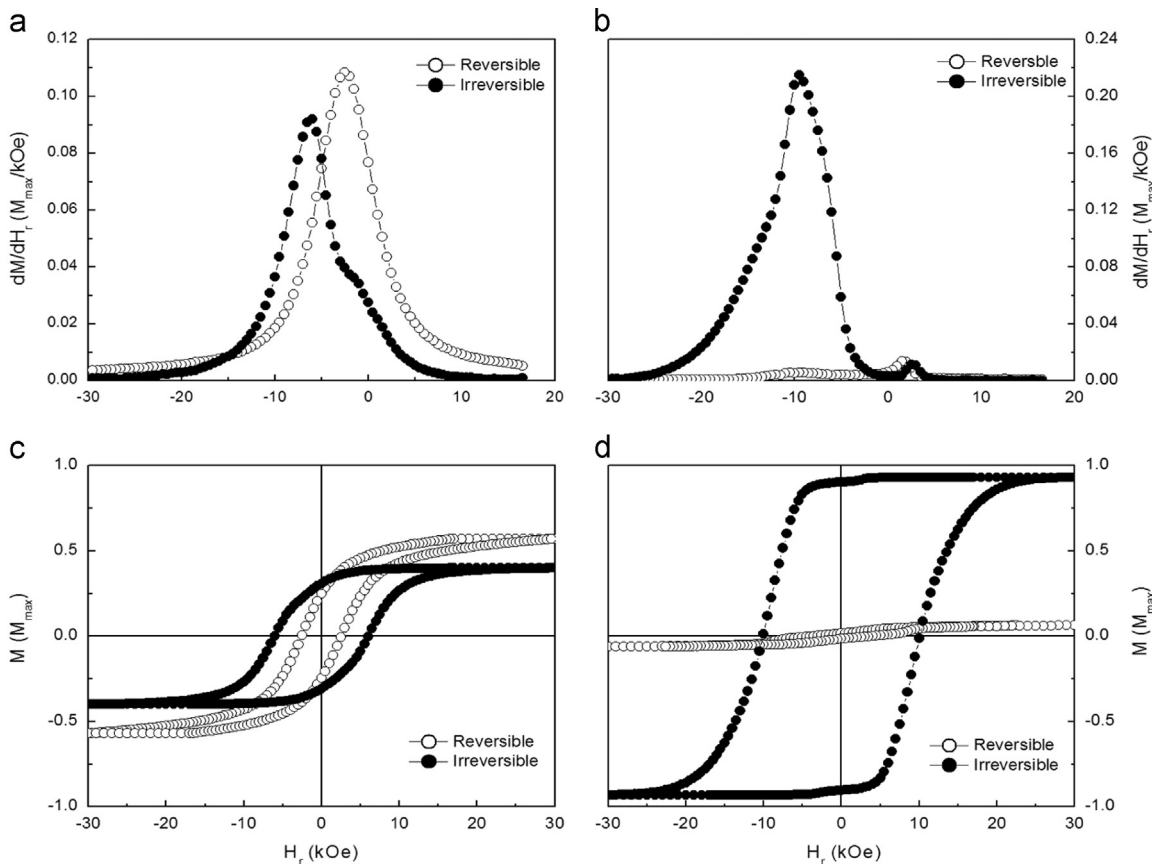
Fig. 6. (a) and (b) show the extracted reversible (open circles) and irreversible (filled circles) distributions of the MQP-B and sintered-NdFeB, respectively. (c) and (d) display purely reversible (open circles) and irreversible (filled circles) hysteresis loops of the MQP-B and sintered-NdFeB, respectively. (a) and (b) share the same horizontal scale in H_r (kOe); the symbol of H_r (kOe) is not presented in (a) and (b) for the purpose of a better figure-combination.
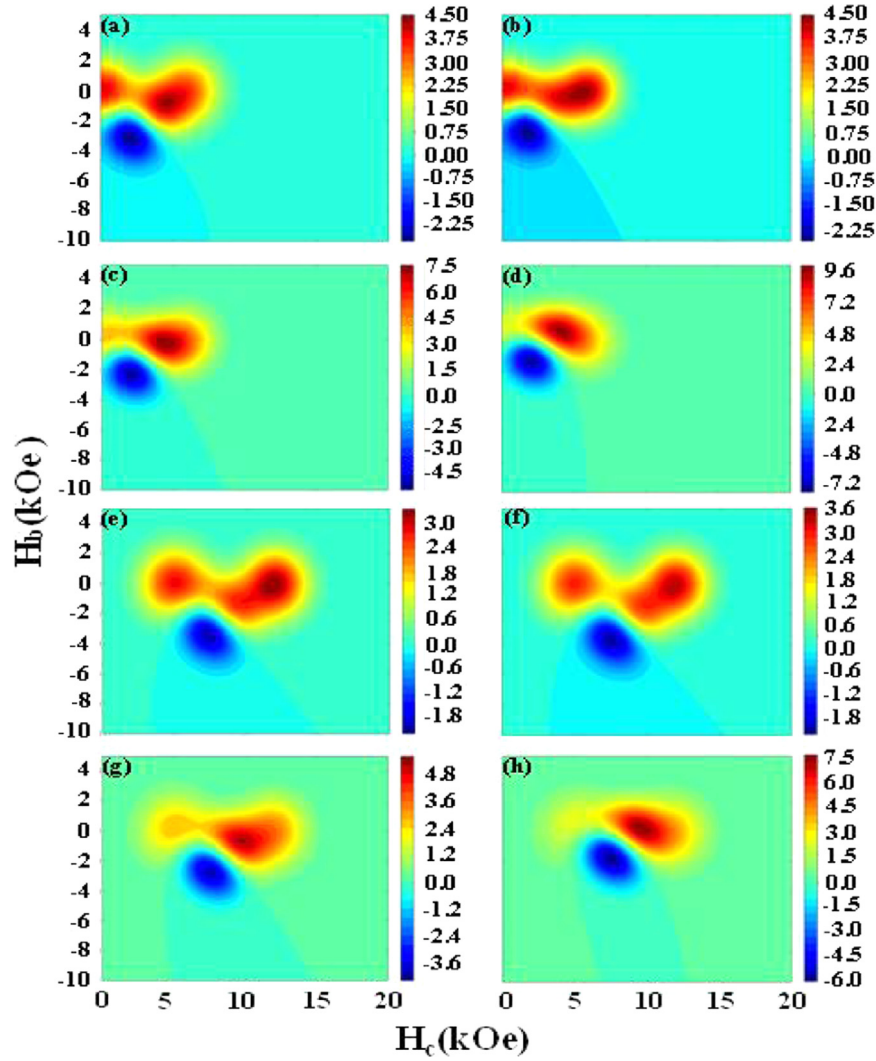
Fig. 7. (a)–(d) are a set of FORCs simulations for the MQP-B with different soft–hard interactions (γ_{HS} and γ_{SH}). (e)–(h) are the other set of FORCs simulations for the sintered-NdFeB, also with different soft–hard interactions. All the sub-figures share the same vertical scale in H_b (kOe) and horizontal scale in H_c (kOe). Simulation details are given in Table 1.

sintered-NdFeB is almost negligible. This indicates that the hysterons of the sintered-NdFeB are extremely stiff and hard to return to the initial state once reversed by an H_r. We notice that the hard component of the sintered-NdFeB is not only dominant but also widespread in H_c, and part of the distribution even exceeds 15,000 Oe. These "stiff" components could have worsened the irreversibility with extremely high magnetic stabilities. For the MQP-B, its soft component appears to extend vertically along the line of near-zero H_c. This feature is similar to the "reversible ridge" obtained in Pike et al. [16], which provides excessive softness favoring the switching reversibility.

We hereby turn focus to the soft–hard coupling. The soft–hard coupling observed in FORCs can be characterized as the intermediate hysterons bridging the tremendous amounts of hysterons bound to the soft and hard components. These intermediate hysterons are more free from the control of the soft/hard components and have more independent responses to an external field. A factor suitable for evaluating the strength of the soft–hard coupling (intermediate hysterons), is the interaction field related to H_b [16]. For the MQP-B (Fig. 3(a)) its soft and hard components are coupled in a way close to zero H_b, suggesting a weak interaction field between the two components. The interaction field is enhanced in the sintered-NdFeB, with the coupling shifting towards the negative H_b region, which could be ascribed to a

strong interaction field between the two components related to the prominent M_s.

However, in a soft–hard coexisting system, the two magnetic counterparts tend to respond to the external field differently. For example, both samples tend to switch the soft component first, and followed by the reversal of the hard component to reach the final state. This results in incoherency during magnetization reversal, which is an undesired nature undermining the magnetic stability. To further understand how the two components interact to mediate the switching coherency, we present a serious of FORCs simulations from Fig. 7(a) to (f) (Fig. 7(a)–(d) corresponds to the MQP-B, and Fig. 7(e)–(h) corresponds to the sintered-NdFeB), using a mean-field approach model proposed by Panagiotopoulos [46]. The model consists of a hard and a soft component. We first simulated the FORCs distributions of the soft and hard components using the following equation:

$$\rho_{S,H}(H_a,\, H_r) = \frac{1}{2\pi\sigma_i^2}\, \exp\left(-\frac{(H_a-H_{ci})^2+(H_r+H_{ci})^2}{2\sigma_i^2}\right)$$

where $\rho_{S,H}$ represents the FORCs of the soft/hard component, σ_i is the width of the Gaussian distribution, and H_{ci} is the hypothetical coercive field of the soft (hard) component. This equation has included the H_c information of the soft and hard components in

the FORCs distribution. In simulation we set the soft and hard H_{ci} to be 150 and 5900 Oe, respectively for the MQP-B, but assigned the soft and hard H_{ci} to be 4700 and 12,800 Oe, respectively, for the sintered-NdFeB. These values were the H_c centers of the soft and hard components estimated from the experimental FORCs data as mentioned above. From the experimental FORCs the two components appear to be comparable for the MQP-B in terms of intensity, but the hard component is superior to the soft one for the sintered-NdFeB. Modifications to the soft (hard)-weighting were therefore tested against the experimental FORCs in the sintered-NdFeB simulations, and we found that a ratio of 1.4 for hard/soft was reasonable. We then simulated the FORC of the interactions between the two components with the equation from Ref. [46] as follows:

$$\frac{\partial^2 m}{\partial H_a \partial H_r} = -\frac{2\gamma}{\pi \sigma_H \sigma_S^3} \left(\frac{H_a + \gamma_{SH} m_H (H_r - \gamma_{HS}) - H_{C,S}}{\sqrt{2}\sigma_S} \right)$$

$$\times \exp\left(-\frac{(H_a + \gamma_{SH} m_H (H_r - \gamma_{HS}) - H_{C,S})^2}{2\sigma_S^2} - \frac{(H_r - \gamma_{HS} + H_{C,H})^2}{2\sigma_H^2} \right)$$

where m_S (m_H) refers to the magnetization of the soft (hard) component, and γ_{HS} (γ_{SH}) is the parameter (with arbitrary unit) referring to the interaction strength that the hard (soft) component exerts on the soft (hard) component. Each component is subjected to a hypothetical magnetic field, which is the sum of the external field plus an extra field proportional to the magnetization of the other component. More details regarding the model setting can be found in Ref. [46]. Using the equation a blue polarity feature is generated, which corresponds to the interactions between the obvious soft and hard components. Compared to the experimental data (Fig. 3) the blue polarity with a negative intensity refers to the perturbed signal arising from the interactions between the two components. In simulations we focus on the values of γ_{HS} and γ_{SH} rather than the shape of the FORCs distribution, as the latter is difficult to control due to many variables of the equation, and the equation mainly emphasizes the interdependency between γ and H_c.

Table 2 lists the calculated γ_{HS}/γ_{SH} for the MQP-B and sintered-NdFeB. For the MQP-B (Fig. 7(a)–(d)), a reasonable simulation is achieved when the mutual interacting forces of the two components are equal and low ($\gamma_{HS} = \gamma_{SH} = 0.1$, Fig. 7(a)). Increasing γ_{HS} to 0.2 while keeping γ_{SH} at 0.1 results in a stronger coupling, with the tendency for the soft component being merged by the hard component (Fig. 7(b)). If both γ_{HS} and γ_{SH} are increased to

0.2 the soft component is merged by the hard one (Fig. 7(c)). A single hard component is present if continuously increasing both γ_{HS} and γ_{SH} to 0.3 (Fig. 7(d)). For the sintered-NdFeB (Fig. 7(e)), γ_{HS} needs to be twice than γ_{SH} to produce FORCs close to the experimental data. This is because of the dominance of the hard component, which naturally exerts a more potent force on the soft counterpart. Lowering both γ_{HS} and γ_{SH} to 0.1 weakens the coupling, with the feature of overlapping becoming marginal. Yet similar to the MQP-B, the FORCs of the sintered-NdFeB becomes singly distributed if equally increasing γ_{HS} and γ_{SH} from 0.2 to 0.3, as one follows from Fig. 7(g) to (h). Through simulations we understand that the soft–hard interaction is only moderate in a real $Nd_2Fe_{14}B$ compound. This moderate interaction split the soft and hard components, leading to reversal incoherency that undermines the magnetic stability. It is a key factor hindering the performance improvement of the $Nd_2Fe_{14}B$ nowadays, because this phenomenon is hard to be detected by conventional magnetic analyses. Ideally, a true "hard" magnetic nature can be achieved if γ_{HS} and γ_{SH} are large and equal. In this situation the soft and hard components are strongly bound together with the annihilations of the intermediate hysterons. This will enable a coherent reversal primarily residing at the hard component, which is expected to effectively promote the magnetic stability of the $Nd_2Fe_{14}B$. This finding adds a new notion to the current available strategies for improving the $(BH)_{max}$ of the $Nd_2Fe_{14}B$ [47–53]. There exists a "trade-off" that in a strong coupling case the merged single hard component sacrifices some magnetic stability by shifting its H_c center to a lower value, but this could be compensated by the enhanced switching coherency.

4. Conclusions

Sophisticated FORCs analyses were performed on the two commercial $Nd_2Fe_{14}B$ to explore the reversal dynamics of the materials beyond traditional magnetization and coercivity information. With this approach soft and hard reversal components were found to present simultaneously in the two samples in spite of distinct properties. The presence of the soft component undermined the magnetic hardness of the $Nd_2Fe_{14}B$. As this material is on high demand in current industry, the found problem needs prompt solutions to foster the related technologies. A moderate soft–hard coupling was obtained in FORCs simulations using the mean-field approach. Theoretically, a coherent reversal can be enabled if the two components exert equal but large interacting forces upon each other. This is expected to output a superior $(BH)_{max}$ than the maximum attainable $(BH)_{max}$ with extrinsic tuning.

Table 2
Simulation parameters using the mean-field-approach for the FORCs simulations presented in Fig. 7.

Sample (figure)	Interaction of HS	Interaction of SH	Deviation of soft component	Deviation of hard component
MQP-B (Fig. 7(a))	0.1	0.1	0.2	0.2
MQP-B (Fig. 7(b))	0.2	0.1	0.2	0.2
MQP-B (Fig. 7(c))	0.2	0.2	0.2	0.2
MQP-B (Fig. 7(d))	0.3	0.3	0.2	0.2
Sintered-NdFeB (Fig.. 7(e))	0.2	0.1	0.2	0.22
Sintered-NdFeB (Fig. 7(f))	0.1	0.1	0.2	0.22
Sintered-NdFeB (Fig. 7(g))	0.2	0.2	0.2	0.22
Sintered-NdFeB (Fig. 7(h))	0.3	0.3	0.2	0.22

References

[1] S. Yamashita, J. Yamasaki, M. Ikeda, N. Iwabuchi, J. Appl. Phys. 70 (1991) 6627.
[2] D.M. Tsamakis, M.G. Ioannides, G.K. Nicolaides, J. Alloys Compd. 241 (1996) 175.
[3] J.F. Herbst, Rev. Mod. Phys. 63 (1991) 819.
[4] D. Haskel D., J.C. Lang, Z. Islam, A. Cady, G. Srajer, M. van Veenendaal, P.C. Canfield, Phys. Rev. Lett. 95 (2005) 217207.
[5] K. Uestuener, M. Katter, W. Rodewald, IEEE Trans. Magn. 42 (2006) 2897.
[6] D.W. Scott, B.M. Ma, Y.L. Liang, C.O. Bounds, J. Appl. Phys. 79 (1996) 5501.

[7] R. Fischer, T. Schrefl, H. Kronmüller, J. Fidler, J. Magn. Magn. Mater. 135 (1996) 35.
[8] R. Zhang, Y. Liu, J. Ye, W. Yang, Y. Ma, S. Gao, J. Alloys Compd. 427 (2007) 78.
[9] Z.W. Liu, H.A. Davies, J. Magn. Magn. Mater. 313 (2007) 337.
[10] J.I. Betancourt R., H.A. Davies, IEEE Trans. Magn. 37 (2001) 2480.
[11] W. Chen, R.W. Gao, M.G. Zhu, W. Pan, W. Li, X.M. Li, G.B. Han, W.C. Feng, B. W. Wang, J. Magn. Magn. Mater. 261 (2003) 222.
[12] F. Vial, F. Joly, E. Nevalainen, M. Sagawa, K. Hiraga, K.T. Park, J. Magn. Magn. Mater. 242 (2002) 1329.
[13] H. Kim, S. Cho, Y. Kim, H. Kim, G.A. Kapustin, J. Appl. Phys. 93 (2003) 8137.
[14] J.W. Kim, S.Y. Song, Y.D. Kim, J. Alloys Compd. 540 (2012) 141.
[15] R. Gholamipour, A. Beitollahi, V.K. Marghusian, T. Ohkubo, K. Hono, S.V. Andreev, A.N. Bogatkin, S.S. Duragin, A.N. Kozolov, N.V. Kudervatykh, Phys. Status Solidi A 203 (2006) 287.
[16] C.R. Pike, C.A. Ross, R.T. Scalettar, G. Zimanyi, Phys. Rev. B 71 (2005) 134407.
[17] R.K. Dumas, C.P. Li, I.V. Roshchin, I.K. Schuller, K. Liu, Phys. Rev. B 75 (2007) 134405.
[18] R.K. Dumas, K. Liu, C.P. Li, I.V. Roshchin, I.K. Schuller, Appl. Phys. Lett. 91 (2007) 202501.
[19] C.R. Pike, A.P. Pobert, K.L. Verosub, J. Appl. Phys. 85 (1999) 6660.
[20] L. Stoleriu, A. Stancu, IEEE Trans. Magn. 42 (2006) 3159.
[21] F. Preisach, Z. Phys. 94 (1935) 277.
[22] G. Bertotti, V. Basso, J. Appl. Phys. 73 (1993) 5827.
[23] C. Rong, Y.Q. Wu, D. Wang, Y. Zhang, N. Poidyal, M.J. Kramer, J.P. Liu, J. Appl. Phys. 111 (1993) 07A717.
[24] H. Chiriac, M. Marinescu, J. Non-Cryst. Solids 287 (2001) 140.
[25] D. Brown, B.M. Ma, Z. Chen, J. Magn. Magn. Mater. 248 (2002) 432.
[26] F. Béron, D. Ménard, A. Yelon, J. Appl. Phys. 103 (2008) 07D908.
[27] F. Béron, J. Clime, M. Ciureanu, D. Ménard, R.W. Cochrane, J. Appl. Phys. 101 (2007) 09J107.
[28] A.R. Muxworthy, A.P. Roberts, Encyclopedia of Geomagnetism and Paleomagnetism, Springer, Netherlands (2007) 266.
[29] C.R. Pike, Phys. Rev. B 68 (2003) 104424.
[30] T. Schrefl, T. Schoji, M. Winklhofer, H. Oezelt, M. Yano, G. Zimanyi, J. Appl. Phys. 111 (2012) 07A728.
[31] D. Saccone, L.G. Pampillo, M.I. Oliva, P.G. Bercoff, H.R. Bertorello, H.R.M. Sirkin, Physica B 398 (2007) 313.
[32] H. Chiriac, N. Lupu, L. Stoleriu, P. Postolache, A. Stancu, J. Magn. Magn. Mater. 316 (2007) 177.
[33] M. Jurczyk, J. Jakubowicz, J. Magn. Magn. Mater. 185 (1998) 66.
[34] G.B. Han, R.W. Gao, S. Fu, W.C. Feng, H.Q. Liu, W. Chen, W. Li, Y.Q. Quo, Appl. Phys. A 81 (2005) 579.
[35] S. Bance, H. Oezelt, T. Schrefl, G. Ciuta, N.M. Dempsey, D. Givord, M. Winklhofer, G. Hrkac, G. Zimanyi, O. Gutfleisch, T.G. Woodcock, T. Shoji, M. Yano, A. Kato,and, A. Manabe, Appl. Phys. Lett. 104 (2014) 182408.
[36] M. Gronefeld, H. Kronmuller, J. Magn. Magn. Mater. 99 (1990) L267.
[37] A. Manaf, M. Leonowicz, R.A. Buckley, H.A. Davies, in: Proceedings of the 7th International Symposium on Magnetic Anisotropy and Coercivity in RE–Transition Metallic Alloys, University of Western Australia, 1992, p. 115.
[38] A. Manaf, P.Z. Zhang, I. Ahmad, H.A. Davies, R.A. Buckley, IEEE Trans. Magn. 29 (1993) 2866.
[39] M. Paunovic, M. Schlesinger, Fundamentals of Electrochemical Deposition (2nd ed.), John Wiley & Sons, p. 164.
[40] P.G. McCormick, W.F. Miao, P.A.I. Smith, J. Ding, R. Street, J. Appl. Phys. 83 (1998) 6256.
[41] R.W. Gao, W.C. Feng, H.Q. Liu, B. Wang, W. Chen, G.B. Han, P. Zhang, H. Li, W. Li, Y.Q. Guo, W. Pan, X.M. Li, M.G. Zhu, X. Li, J. Appl. Phys. 94 (2003) 664.
[42] Z. Zhang, P. Sharma, K. Yubuta, A. Makino, J. Appl. Phys. 111 (2012) 07B501.
[43] M. Leonowicz, M. Spyra, E. Jezierska, Mech. Adv. Mater. Struct. 18 (2011) 181.
[44] M. Yamada, H. Kato, H. Yamamoto, Y. Nakagawa, Phys. Rev. B 38 (1988) 620.
[45] M. Winkhofer, R.K. Dumas, K. Liu, J. Appl. Phys. 103 (2008) 07C518.
[46] I. Panagiotopoulos, J. Magn. Magn. Mater. 323 (2011) 2148.
[47] D.W. Scott, B.M. Ma, Y.L. Liang, C.O. Bounds, J. Appl. Phys. 79 (1996) 4830.
[48] B.E. Davies, R.S. Mottram, I.R. Harris, Mater. Chem. Phys. 67 (2001) 272.
[49] S. Pandian, V. Chandrasekaran, G. Markandeyulu, K.J.L. Iyer, K.V.S. Rama Rao, J. Appl. Phys. 92 (2002) 6082.
[50] G. Xie, S. Yin, F. Zhang, P. Lin, B. Gu, M. Lu, Y. Du, Z. Yuan, Mater. Lett. 58 (2004) 636.
[51] G. Bai, R.W. Gao, Y. Sun, G.B. Han, B. Wang, J. Magn. Magn. Mater. 308 (2007) 20.
[52] W. Li, L. Li, Y. Nan, X. Li, X. Zhang, D.V. Gunderov, V.V. Stolyarov, A.G. Popov, Appl. Phys. Lett. 91 (2007) 062509.
[53] M. Pan, P. Zhang, X. Li, H. Ge, Q. Wu, Z. Jiao, T. Liu, J. Rare Earth 28 (2010) 399.